Determination of hydrogenated amorphous silicon electronic transport parameters and density of states using several photoconductivity techniques

C. Longeaud,[1] F. Ventosinos,[2] and J. A. Schmidt[2]
[1]*Laboratoire de Génie Electrique de Paris (CNRS UMR 8507), Plateau de Moulon, 11 rue Joliot Curie, 91190 Gif sur Yvette, France*
[2]*INTEC (UNL-CONICET), Güemes 3450, 3000 Santa Fe, Argentina*

(Received 29 December 2011; accepted 2 July 2012; published online 27 July 2012)

In this paper, we show that the combination of different characterization techniques based on the photoconductivity of hydrogenated amorphous silicon can be a tool to investigate on the density of states and transport parameters of this material. We insist mainly on two techniques in which one records a photocurrent resulting from the movement of an interference grating onto a sample. We describe the experimental set-ups and provide a theoretical explanation of the observed behaviors of these photocurrents. We demonstrate that a density of state spectroscopy can be done with these techniques. Additionally, comparing this spectroscopy to that performed with modulated photocurrent experiment, we show that it is possible to derive a good order of magnitude estimate of the electron capture coefficient of the conduction band tail states as well as the electronic extended states mobility. The derived parameters are compared with previous results. © *2012 American Institute of Physics*. [http://dx.doi.org/10.1063/1.4737790]

I. INTRODUCTION

Hydrogenated amorphous silicon (a-Si:H) being one of the major thin film materials used for solar energy conversion, much research has been involved in measuring its transport parameters to optimize the deposition conditions and its properties. Determination of the density of localized states (DOS) distribution has been one of the topics of these investigations, and many techniques have been proposed, using the photoconductivity properties of the studied material. For the four techniques considered in this paper the samples were built in coplanar geometry by deposition on glass substrates and fitted with two parallel and ohmic electrodes. The simplest one is the steady state photoconductivity (SSPC) in which the part of the sample in between the biased electrodes is maintained at a given temperature and uniformly illuminated by a steady flux of light, the wavelength of which is chosen to provide band to band generation.[1–3] A time component can be added to the SSPC experiment either by studying transient photoconductivity after the light is switched off[4] or by modulating part of the flux at an angular frequency ω that results in the modulated photocurrent (MPC) technique.[5–7] On the other hand, a spatial distribution of light in between the electrodes under steady illumination provides information on the minority carrier diffusion length, this technique being known as the steady state photocarrier grating (SSPG).[8] Again, a time component can be added to this latter technique, either by modulation of the grating,[9] or with a grating moving at a constant speed (the moving grating technique, MGT),[10] or even with a grating oscillating at an angular frequency ω (the oscillating photocarrier grating technique, OPG).[11] In the last two cases, the measurements can be performed without applying an external electric field to the sample. All these techniques can provide pieces of information on the studied material, but a combination of them can give a deeper insight into its transport properties.

For instance, SSPC was used to derive an order of magnitude of the characteristic temperature of the a-Si:H conduction band tail[1] or a DOS map in micro-crystalline silicon with the help of numerical simulations.[2] We would like to underline that the MPC technique offers the possibility to achieve a DOS spectroscopy in two different regimes depending on ω, called low frequency (LF-MPC) and high frequency (HF-MPC) regimes. However, the energy scaling of the spectroscopy in these two regimes can be done accurately only if the extended states mobility and the capture coefficients of the probed states are known, respectively. In an earlier paper,[12] we compared and combined the results coming from SSPC, HF-MPC, and LF-MPC and showed that, in addition to the DOS spectroscopy, one can deduce from these experiments orders of magnitude of the electron extended states mobility and the capture coefficients of the probed states.

In this paper, we propose to combine the SSPC, HF-MPC (that we shall call simply MPC in the following), MGT, and OPG techniques, showing that their application to the a-Si:H study leads also to an accurate DOS spectroscopy as well as to the determination of electron conduction band tail capture cross section and extended states mobility. As far as the conduction band tail is concerned, we shall show that MGT and OPG techniques are good alternative techniques to the LF-MPC experiment.

SSPC and MPC techniques are rather well-known and have been described in the literature.[1–7] Therefore, we shall not detail them in this paper. The two other techniques, MGT and OPG, have not received as much attention. That is why, in the first part of this paper, we shall recall the bases of these techniques, show and explain that they provide

basically the same information, though with peculiar advantages and drawbacks that make them complementary, and that a DOS spectroscopy can be achieved with them. In a second part, we shall show how to combine all these techniques to derive an accurate DOS spectroscopy as well as transport parameters. We shall also compare the parameters we obtained on different samples with those we have previously found.[12,13]

II. EXPERIMENTAL SET-UP FOR THE MGT AND OPG TECHNIQUES

The experimental set-up used for both techniques is shown in Fig. 1. The light source is a He-Ne laser, the wavelength of which satisfies two requirements: a photon energy (1.96 eV) slightly larger than the a-Si:H band gap and a rather uniform absorption through the thickness of the samples ($\sim$0.5 μm). The laser light, linearly polarized in the vertical direction, is split into two coherent beams that finally interfere at the sample position. One of the beams, attenuated by a neutral density filter to an intensity I_2, impinges the sample perpendicularly, while the other one, of intensity $I_1 \gg I_2$, forms an angle δ with the former beam. Therefore, an intensity grating with a spatial period $\Lambda = \frac{\lambda}{\sin(\delta)}$ is created, where λ is the light wavelength. In the MGT technique, two acousto-optic modulators (AOM) are used to introduce a small frequency shift Δf between the light frequencies of the beams, which causes the intensity grating to move parallel to the sample surface with a constant velocity proportional to Δf. The resulting illumination intensity is found to be

$$I = I_0 + \delta I \cos[k\,(x - v_{gr}\,t)], \tag{1}$$

where $I_0 = I_1 + I_2$, $\delta I = 2\sqrt{I_1 I_2}$, $v_{gr} = \Lambda \Delta f$, and $k = \frac{2\pi}{\Lambda}$.[10] The dc short circuit current, resulting from the movement of the intensity grating, is measured with an electrometer. Prior to these measurements, one has to verify that the contacts are ohmic to check that no built-in field at the contacts would alter the short circuit current data.

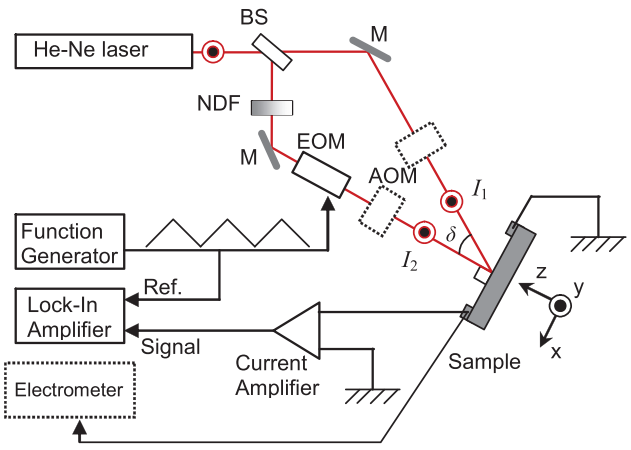

FIG. 1. Experimental setup for the experiments. A linearly polarized laser beam is split by a beam splitter (BS) into two beams, I_1 and I_2, which are made to coincide on the sample by using the mirrors (M). Beam I_2, attenuated by a neutral density filter (NDF), passes through an electro-optic modulator (EOM) used as a phase modulator (OPG technique); or both beams go through acousto-optic modulators (AOM, MGT technique) to obtain a small shift in their frequencies. The lock-in amplifier measures the ac photocurrent due to the oscillating grating, whereas the electrometer is used to read the dc current generated in MGT configuration.

In the OPG technique, the two acousto-optic modulators are replaced by a single electro-optic modulator (EOM) used to control the phase of beam I_2, while beam I_1 remains unaltered. In order to control the phase of beam I_2, the EOM is positioned with the axes of the crystal vertical and horizontal. In this "phase modulation" configuration, the output amplitude and polarization remain unchanged, but the phase of the wave can be varied as a function of the signal applied to the modulator. When this function is a triangular wave function, the calculation of the resulting illumination intensity impinging the sample gives[11]

$$I = I_0 + \delta I \cos(k\,x \pm \omega\,t), \tag{2}$$

where ω is the angular frequency of the triangular wave and the other symbols have the same meaning as before. The result is an intensity grating that moves with a constant velocity in one direction for the first half of a period (therefore for half a grating period) and then moves in the opposite direction for the second half of a period. In this way, OPG can be seen as an ac version of MGT, the current being measured with a lock-in amplifier, and therefore should provide a better signal to noise ratio compared to MGT.

III. EXPERIMENTAL MEASUREMENTS

As mentioned in Sec. II, both techniques have a common origin, which is a grating moving over the sample. For the MGT technique, the grating is moving in one direction at a constant speed, whereas for the OPG the grating is moving at a constant velocity on one direction during the first half of a period of the signal driving the EOM and at a constant velocity toward the other direction during the second half of a period. Therefore, we expect to find similar behaviors for the measured excess current in both techniques. This property can be used to explore the material response on a large range of operational conditions, since the accuracy of OPG and MPG techniques depends on the experimental conditions as explained below.

Experiments were performed on 0.5 μm thick samples deposited onto glass substrates by radio frequency (13.5 MHz) powered plasma enhanced chemical vapour deposition at a temperature of 190 °C. The electrodes were made of parallel strips of silver paste, 1 mm apart and 1 cm long. For these two techniques, no bias was applied in between the electrodes (short-circuit conditions). To check for an influence of possible built-in fields close to the electrodes, we have first verified that the electrodes were ohmic in a large range of biases (0–100 V), and we also performed MGT measurements with the grating moving in one direction and then the other. We did not observe sensible differences between both MGT curves, and under each condition, the maximum was found at the same position. Therefore, we concluded that the contact potentials, if any, had no influence on our measurements.

Figure 2 displays the evolution of the excess current measured *under short circuit conditions* on the same sample

as function of the difference in frequencies (MGT) or of the EOM driving frequency (OPG), for different temperatures indicated in the inset. The grating period was $\Lambda \approx 5\ \mu$m, and the ratio of the two beam fluxes was fixed to 20. In this figure, it is clear that both techniques give the same excess current evolution for the same temperatures, $T = 220$ and 250 K.

However, for lower temperatures, the excess current is very small, of the order of a few pA, and turns to be very difficult to record accurately even with an electrometer. Nevertheless, given the fact that OPG uses a current/voltage amplifier and a lock-in amplifier, small values of photocurrent can still be measured for low temperatures. Therefore, OPG appears to be the most suitable technique when the signal level is low, as shown in Fig. 2 for $T = 170$ K.

On the other hand, as can be seen in Fig. 2, an increase in the temperature results in a shift of the maximum of the curves towards higher frequencies. At these frequencies, the bandwidths of the current/voltage amplifier and of the lock-in amplifier start to limit the applicability of the OPG technique, whereas the increase of the excess current makes the dc current easier to measure. Hence, the MGT seems to be a more suitable method for high temperatures, as shown in Fig. 2 for $T = 300$ K.

The same experiments were also performed at different photon fluxes keeping constant the temperature.[14] The variation of the photon flux causes a similar effect as the variation of the temperature. For low generation rates, OPG is best suited because of the small currents involved. Increasing the photon flux, a range of fluxes appears where both techniques can be used, and for high generation rates, MGT is more appropriate because it avoids the bandwidth limitations of OPG.

These results show that both techniques are complementary, not because they provide different information on the studied material but because the use of both techniques extends the range of accessible frequencies and temperatures, leading to a wider domain of investigation. Indeed, one can choose the method that is best adapted to the temperature/photon flux conditions under which the measurements are done. However, these experimental results need to be explained before more information can be extracted from them. In Sec. IV, we shall clarify why an excess current can be measured the sample being short circuited, why both techniques are leading to the same behavior and underline the origin of the bell-shape curves we obtain. We shall insist on the origin of the maximum of these curves and finally show that the knowledge of this maximum opens the possibility to perform a DOS spectroscopy.

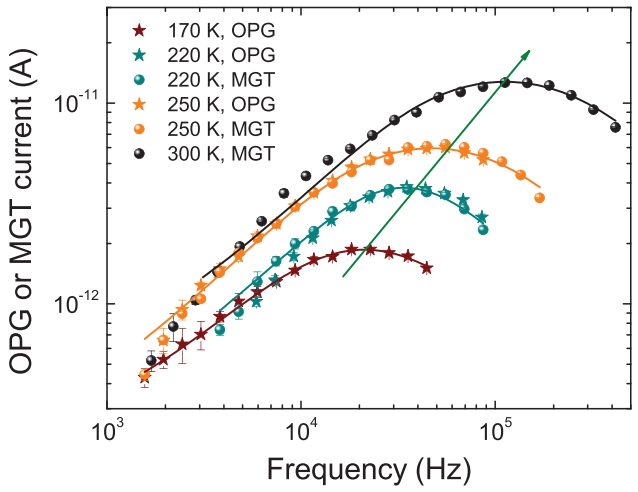

FIG. 2. Measurements of OPG (stars) and MGT (circles) techniques, performed for four different temperatures. As can be seen, there is a range of temperatures where both techniques can be used, giving the same results. For lower temperatures, the photoconductivity is too low to be measured by an electrometer. For higher values, the OPG has bandwidth limitations. The lines are fits with Eq. (18), while the arrow indicates the shift of the maximum.

IV. THEORETICAL BACKGROUND AND DOS SPECTROSCOPY

Though the basic principles of the calculation of the excess current density $\delta J(\omega)$ measured with the OPG or MGT experiment have been already presented elsewhere,[11] we give in the Appendix a more detailed calculation. This calculation starts from the continuity equation for electrons and holes along with the Poisson equation. From these equations, one can calculate the final expression of $\delta J(\omega)$, assuming that the attenuated beam creates only a small perturbation of the steady state of the sample fixed by the main beam. These equations were also introduced into numerical calculations from which, after introducing DOS distributions and parameters, we could study the evolution of the OPG and MGT currents with the frequency, temperature, and flux for different transport parameters.

As can be seen in Fig. 2, a clear maximum appears on the curves $\delta J(\omega)$ that can be explained in the following way. The light grating impinging on the sample creates several arrays, in particular, an array of free carriers $n(x)$ and an array of trapped carriers $N_{trap}(x)$. With a large Λ, $N_{trap}(x)$ does not vanish by diffusion and eventually creates a space charge array that results in an internal electric field array $\xi_{int}(x)$. With a static grating, as in the SSPG technique, $n(x)$ and $\xi_{int}(x)$ are in quadrature, implying that the current is null without an external electric field. When the light array is moving along the film surface with a relatively low velocity, the free carriers grating follows it almost instantaneously, whereas the space charge array lies behind due to the necessary delay the trapped carriers need to reorganize. The $n(x)$ and $\xi_{int}(x)$ arrays are no longer in quadrature, and a current may appear from the movement of free carriers (mostly electrons in a-Si:H) in the internal field, which occurs even though the external field $\xi_{ext} = 0$ V/cm. With a low external electric field applied, the alternating current is still mainly due to the internal field, and we have obtained the same variations of δJ vs. ω as with zero field applied.[11]

As ω increases the velocity of the light grating increases too, and the phase lag between $n(x)$ and $\xi_{int}(x)$ tends to decrease, resulting in a steady increase of the OPG or MGT currents. However, if the time needed for the light to cover a distance Λ becomes too small, the trapped charges do not have time to reorganize and to follow the light array. The space charge array starts to blur, and the result is a decrease

of the local internal field. The competition between the decrease of the phase shift between $n(x)$ and $\xi_{int}(x)$, and the blurring of the space charge, eventually ends with a decrease of the OPG or MGT current density with increasing ω.

The above explanation of the $\delta J(\omega)$ behaviour is of course reflected in its expression given in the appendix (Eq. (A17)). This expression shows that even with no applied external field one should measure a current flowing in the sample because of the movement of free carriers in the internal field as underlined above. Besides, from Ref. 7, it can be seen that the square of the MPC conductivity, σ^2_{mpc}, is the ratio of a constant divided by a second order polynomial in ω. Therefore, Eq. (A17) is similar to a band-pass filter equation: $\delta J(\omega)$ tends toward zero for very small or very large ω and must present a maximum somewhere in between.

This maximum of the $\delta J(\omega)$ curve, obtained for ω_{max}, must be linked to a characteristic time of the material. Several characteristic times can be considered: the dielectric relaxation time τ_{diel}, the free electron lifetime τ_n, and the small signal lifetime τ'_n, that is, the lifetime of the small excess of free plus trapped electrons.[15] To find out to which time corresponds the maximum of the $\delta J(\omega)$ curve, we have used numerical calculations that simulate the OPG technique. In these simulations, we have introduced a typical a-Si:H DOS made of two band tails and deep defects represented by two Gaussian distributions of monovalent states. As a matter of example, the expression of the conduction band tail (CBT) DOS was

$$N(E) = N(E_c)\exp\Big(-(E_c - E)\Big/k_B T_c\Big), \tag{3}$$

where E_c is the energy of the conduction band edge, k_B the Boltzmann constant, and T_c the characteristic temperature of the conduction band tail.

We have reproduced all the experimental behaviours, as those displayed in Fig. 2, and we were also able to determine all the characteristic times and compare them to $1/\omega_{max}$. We present in Fig. 3 the variations of these times with the generation rate G_0. At low generation rates, we observe that $1/\omega_{max}$ is close to τ_{diel} whereas at high generation rates $1/\omega_{max}$ is close to τ'_n. These two cases correspond to the well-known dielectric and lifetime regimes and the transition between them is indicated by a vertical dashed line in Fig. 3.

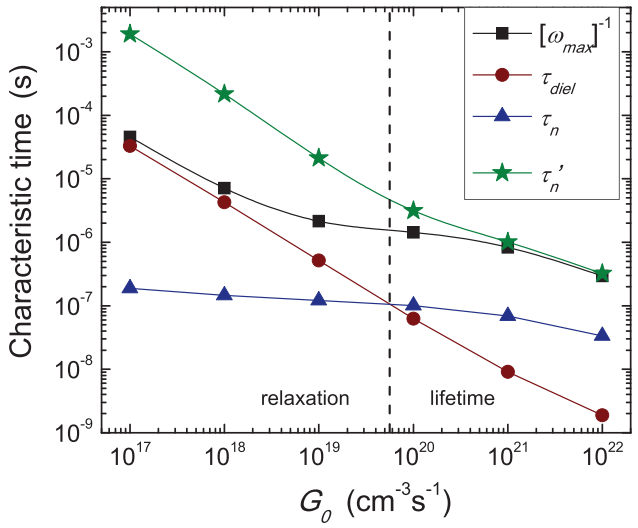

FIG. 3. Calculated results showing the evolution of different characteristic times with the generation rate G_0. The dashed line indicates the transition between the dielectric (left) and recombination (right) regimes.

The knowledge of τ'_n is very interesting because, since this time is linked to the trapped carriers, we expect to extract information on the DOS from it. An expression of τ'_n is[15]

$$\tau_n{}' = \frac{\partial n^{tot}}{\partial G_0} = \frac{\partial\left[n + \int f_0 N^{ACC}\, dE\right]}{\partial G_0}, \tag{4}$$

in which n^{tot} is the total concentration of electrons, i.e., the free (n) plus trapped concentrations, f_0 the occupation function, and N^{ACC} the density of acceptor states (negative when occupied). Operating with Eq. (4) we obtain

$$\tau_n{}' = \frac{\partial n}{\partial G_0} + \int \frac{\delta f_0}{\delta E_{Fn}} \frac{\delta E_{Fn}}{\delta G_0} N^{ACC}\, dE, \tag{5}$$

where E_{Fn} is the electron quasi-Fermi level. In the following, we will assume an n-type semiconductor for which $n \gg p$, thus E_{Fn} can be calculated for from[11]

$$E_c - E_{Fn} = k_B T \ln\left[\frac{q\mu_n N_C}{\sigma_0}\right], \tag{6}$$

where q is the electron charge, N_c is the equivalent density of states at the conduction band edge, and σ_0 the photoconductivity with a generation rate G_0. Taking account of the power-law relationship between photoconductivity and G_0, $\sigma_0 \propto G_0{}^{\gamma}$, a straightforward calculation leads to

$$\frac{\partial n}{\partial G_0} = \frac{\gamma\, n}{G_0}, \quad \frac{\partial E_{Fn}}{\partial G_0} = \frac{\gamma\, k_B T}{G_0}. \tag{7}$$

The occupation function under illumination can be written[16]

$$f_0(E) = \frac{c_n n + e_p}{c_n n + e_p + c_p p + e_n}, \tag{8}$$

where c_n (c_p) and e_n (e_p) are the electron (hole) capture coefficient and emission rate, respectively. In the proximity of E_{Fn}, after some simplifications assuming that $n \gg p$ and that e_p is negligible, one ends with

$$f_0 \cong \frac{1}{1 + \exp\left(\dfrac{E - E_{Fn}}{k_B T}\right)}. \tag{9}$$

Therefore,

$$\frac{\partial f_0}{\partial E_{Fn}} \cong \frac{1}{k_B T} \frac{\exp\left(\dfrac{E - E_{Fn}}{k_B T}\right)}{\left[1 + \exp\left(\dfrac{E - E_{Fn}}{k_B T}\right)\right]^2}. \tag{10}$$

This function presents a sharp maximum at $E = E_{Fn}$ and a full width at half maximum of the order of 3.6 $k_B T$.

Therefore, it can be replaced by a Dirac-delta function, provided $N^{ACC}(E)$ changes with energy with a slope smaller than $1/k_BT$, and, after substitution of Eqs. (7) and (10) into Eq. (5), it leads to

$$\tau_n' \cong \frac{\gamma\, n}{G_0} + \frac{\gamma\, k_B T}{G_0}\int \delta(E - E_{Fn})\, N^{ACC}(E)\, dE$$
$$= \frac{\gamma}{G_0}\left[n + k_B T\, N^{ACC}(E_{Fn})\right], \tag{11}$$

a "classical" approximate expression.[3] As usually done in disordered semiconductors where the density of trapped carriers is much larger than the density of free carriers, we can neglect n in Eq. (11), obtaining

$$N^{ACC}(E_{Fn}) \cong \frac{G_0\, \tau_n'}{\gamma\, k_B T}. \tag{12}$$

Eq. (12) coupled with Eq. (6) allows a DOS spectroscopy if the experiment is performed at different temperatures.

Calculations of τ_n' and γ were achieved with our simulations for temperatures ranging from 100 to 460 K with a generation rate $G_0 = 10^{21}\,\mathrm{cm^{-3}\,s^{-1}}$. The OPG-DOS spectroscopy based on the simplified Eq. (12) is displayed in Fig. 4 (circles), where the general trends of the original DOS (displayed by full lines) are well reproduced, but the precision is rather poor.

When one deals with materials such as a-Si:H, in which the band tails are assumed to decrease exponentially with energy, the OPG/MGT-DOS spectroscopy of the band tail states can be refined if one calculates more accurately the integral of Eq. (4). For that purpose, we shall use the CBT analytical expression [Eq. (3)], and the very good approximation for the occupation function presented before [Eq. (9)]. The concentration of trapped electrons in the conduction band tail is therefore

$$N_{trap} = \int \frac{N(E_c)\exp\left(-\dfrac{E_c - E}{k_b T_c}\right)}{1 + \exp\left(\dfrac{E - E_{fn}}{k_b T}\right)} dE, \tag{13}$$

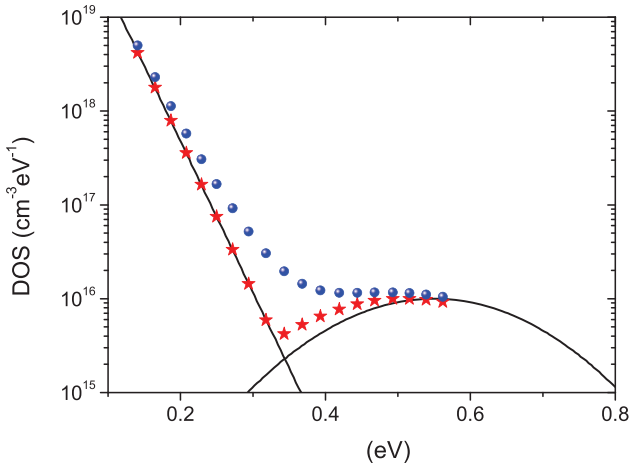

FIG. 4. DOS spectroscopy from the OPG or MGT techniques with a simple procedure (circles) or after correction (stars). Full lines display the original DOS.

where if $T < T_c$, the integral can be taken from $-\infty$ to $+\infty$ without making a large error. Derivation of N_{trap} with respect to E_{fn} gives, after simple calculations,

$$\frac{\partial N_{trap}}{\partial E_{fn}} = N_{trap}(E_{fn})\int \frac{\exp(x\alpha)}{[1 + \exp(x)]^2} dx, \tag{14}$$

writing $x = (E - E_{fn})/k_bT$, and $\alpha = 1 + {}^{T}/_{T_c}$. If α is lower than 2, for temperatures lower than T_c, the integral is equal to $\frac{(1-\alpha)\pi}{\sin(\alpha\pi)}$, giving a refined expression for the DOS in the CBT

$$N^{CBT}(E_{Fn}) = \frac{G_0\, \tau_n'}{\gamma\, k_B T}\frac{(1-\alpha)\pi}{\sin(\alpha\pi)}. \tag{15}$$

Consequently, for measurement temperatures below say 200 K (T_c is believed to be larger than 250 K for device-grade a-Si:H), we can imagine a recurrent procedure to determine the shape of the band tail: extract an order of magnitude of T_c from the OPG/MGT-DOS values obtained by the simple treatment and correct these values with the above expression, check if the final T_c determined from the corrected values of the OPG/MGT-DOS is the same as the introduced one and repeat this procedure until there is a convergence toward the CBT shape. For higher measurement temperatures, we can use this shape to numerically calculate the integral of Eq. (13) and subtract this contribution to the total contribution of the trapping states estimated by means of Eq. (12). Following this procedure, we find the OPG/MGT-DOS displayed by stars in Fig. 4, for which the agreement with the introduced DOS is excellent.

We can compare this DOS spectroscopy with the DOS spectroscopy achieved with MPC. In this experiment, one obtains the quantity Nc_n/μ_n (Ref. 7)

$$\frac{N(E_\omega)c_n}{\mu_n} = \frac{2}{\pi k_B T} qG_{ac}\frac{\sin\phi}{|\sigma_{ac}|}, \tag{16}$$

where $N(E_\omega)$ is the DOS at the energy E_ω, $|\sigma_{ac}|$ the modulus of the photoconductivity resulting from G_{ac}, and ϕ its phase shift referred to the excitation. This quantity Nc_n/μ_n is completely known from experimental data and can be plotted as function of the energy, which is scaled with

$$E_c - E_\omega = k_B T \ln\left[\frac{c_n N_C}{\omega}\right], \tag{17}$$

where ω is the angular frequency of the modulation. The probed DOS being the same in all the experiments considered here, at least in the conduction band tail region, the adjustment of the densities [Eq. (12) or (15) and (16)] and energy scaling [Eqs. (6) and (17)] found in each technique should lead to the determination of $N(E)$, c_n and μ_n independently. Indeed, for all the techniques, it is possible to choose experimental conditions such that they probe the CBT states. From the OPG/MGT techniques one obtains N values, either from the simple or the "refined" procedure, distributed along the energy axis following Eq. (6) in which μ_n is an important parameter. From the MPC technique, one obtains Nc_n/μ_n scaled on the energy axis by means of Eq. (17) in which c_n is the main parameter. The adjustment of the DOS spectra

playing with c_n and μ_n to eventually end with a single DOS distribution, as expected, may lead to a good estimate of $N(E)$, c_n and μ_n (assuming a value for N_c that can be taken equal to that of crystalline silicon at first approximation).

V. DOS SPECTROSCOPIES AND TRANSPORT PARAMETERS IN a-Si:H

The samples studied in this section were the same as those described in Sec. III. The OPG and MPG experiments being performed with large fluxes (to ensure being in the lifetime regime, see Fig. 3), the samples were light-soaked before measurements to avoid evolution of the DOS while measuring it. The accelerated light-soaking was achieved during more than 50 h at 80 °C under red light with a flux of 300 mW/cm^2. Subsequently, for all the experiments, samples were set onto the cold finger of a cryostat under dynamically pumped vacuum (10^{-5} Torr).

The MPC experiment was carried out with red light (at 650 nm) with a dc flux of 10^{14} cm^{-2} s^{-1} and an ac flux three times lower. The applied bias was 100 V. The temperature was varied from 390 K down to 110 K each 20 K and at each temperature the frequency f of the modulation was varied from 12 Hz to 40 kHz in a way such that $f_{i+1} = f_i \times 1.5$. The maximum temperature was chosen so as to have no annealing of the sample during the experiment.

The OPG and MGT experiments were carried out with a He-Ne laser, the flux of the main beam impinging the sample being equal to 1.5×10^{17} cm^{-2} s^{-1}, the other beam being attenuated by a factor of 20. The grating period was of the order of 5 μm. Despite the use of a lock-in amplifier in the OPG technique or currents largely above the detection limits of the electrometer in the MGT technique, the correct detection of a maximum of the $\delta J(\omega)$ curve can be problematic or simply inaccurate because of noise or simply because the measured points at different frequencies do not draw clearly the maximum position. To solve this problem, we used curve fitting. Indeed, as shown in the description of Sec. IV, the system behaves exactly as a band pass filter. Therefore, we have chosen to fit the $\delta J(\omega)$ curve following

$$\delta J(\omega) = \frac{\delta J_{\max}}{\sqrt{1 + Q^2\left[\frac{\omega_{\max}}{\omega} - \frac{\omega}{\omega_{\max}}\right]^2}}, \qquad (18)$$

where δJ_{max}, ω_{max}, and Q correspond, respectively, to the maximum values of the current and angular frequency and of the "quality factor" of the band pass filter. All these quantities have been estimated from the experimental results and have been introduced as an input for a standard least-squares fitting algorithm, from which a rather precise value for ω_{max} has been extracted. We would like to insist on two points. First, the above expression can be considered valid for fitting only in the case where $\omega\tau_D$ is much lower than one. If this is not the case, according to Eq. (A17), the order of the equivalent band pass filter would be higher, and Eq. (18) would not be convenient anymore. Second, Eq. (18), when it can be used, is only a help, or a guide, to refine the determination of ω_{max}. Indeed, the links between Q and some material parameters are far too complex to extract any valuable information from the Q values we have obtained.

At low temperature, the measurements were performed each 10 K using the OPG technique because of the small amplitude of the signal. For temperatures above 250 K, measurements were performed each 20 K. In the temperature range of 250–300 K, both techniques were used, leading to the same results. Above 300 K, only the MGT would give appropriate results, the frequency of the maximum of the $\delta J(\omega)$ curves being at the border of or even well above the band width of the lock-in amplifier. The γ coefficient was calculated at each temperature from the measurements of the SSPC currents with a flux I and a flux $I/2$.

We present in Fig. 5 the DOS spectroscopies achieved with the different techniques. The OPG/MGT-DOS was calculated both from the approximate expression given by Eq. (12) (circles) or by means of the refined expression of Eq. (15) (stars). This last expression is valid only when probing the conduction band tail, and among all the measured points only the first 7 points measured at low temperatures ($T < 190$ K) seem to fulfil this condition. Concerning the MPC, the spectra obtained at different temperatures are depicted by solid lines. We should recall that the DOS shape is given by the upper envelop of the MPC spectra. The deviations from it result from an influence of the mean dc flux used to perform the experiment as described elsewhere.[7] According to Eq. (16), the MPC experiment provides the Nc/μ values. Therefore, to match the different DOS spectroscopies we have varied the c_n and μ_n values. To do so, we have adjusted the N values, either directly obtained from OPG/MGT or calculated form MPC, as well as the energy scaling with Eqs. (6) and (17), to eventually obtain the best agreement between both sets of data. The α value in $\frac{(1-\alpha)\pi}{\sin(\alpha\pi)}$ was also adjusted so that the final data for the first 7 points measured by OPG fit onto an exponential distribution corresponding to the conduction band tail

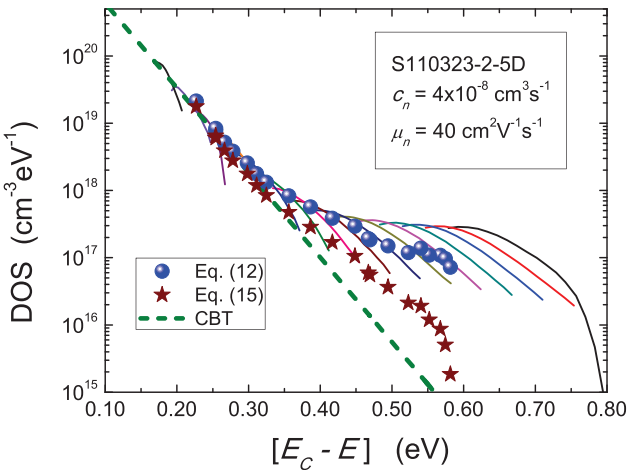

FIG. 5. DOS spectroscopies achieved with the MPC technique (solid lines), the simplified equation for the OPG/MGT techniques (circles) and the "refined" calculation (stars). The straight line represents the conduction band tail distribution exponentially decreasing with a characteristic temperature equal to 400 K. The values of c_n and μ_n that match the DOS distributions are displayed in the figure.

distribution with a characteristic temperature of 400 K (straight line).

We would like to mention that in the present case all the data measured with OPG/MGT could be and were treated by means of Eq. (15). However, for $T > 200$ K, OPG/MGT techniques are probing deep states that are not varying exponentially, which is one of the requirements for Eq. (15) to be applicable, and the final DOS spectroscopy, displayed by stars in Fig. 5, is clearly far from what one would have expected according to the MPC results. This result underlines the fact that Eq. (15) should be used very cautiously and that Eq. (12) is certainly more appropriate to derive a DOS spectroscopy, as far as deep states are concerned. The reader shall also note that we have not strictly followed the refined procedure described in Sec. IV, subtracting the CBT contribution to the deep states distribution estimated from Eq. (12). It would have loaded the figure without bringing much more information.

The value of the characteristic temperature of the conduction band tail seems to be rather high since one would expect an order of magnitude of $T_c \approx 300$ K. However, we have shown in a previous paper that light-soaking resulted both in an increase of the deep defect density and in a widening of the conduction band tail.[17] Since we are dealing with light-soaked sample, a T_c of the order of 400 K seems to be a reasonable value.

The adjustment of the different curves, in the CBT region, leads to $c_n = 4 \times 10^{-8}$ cm^3 s^{-1} for the CBT states and $\mu_n = 40$ cm^2 V^{-1} s^{-1}, assuming a value of the equivalent density of states of the conduction band equal to that of crystalline silicon, $N_c = 2.5 \times 10^{19}$ cm^{-3} at room temperature. These values are in good agreement with previous measurements combining the MPC measurements in the high and in the low frequency regimes,[13] measurements from which we had found $c_n = 2.5 \times 10^{-8}$ cm^3 s^{-1} and $\mu_n = 50$ cm^2 V^{-1} s^{-1}. Hence, OPG/MGT provides an alternative and/or complementary mean to derive these parameters.

Considering the adjustment between the MPC spectra and the OPG/MGT data for $(E_C\text{-}E) \geq 0.45$ eV, it is clear that the DOS points obtained from MPC and from Eq. (12) applied to the OPG/MGT data do not agree. The reason is that for the plot of Fig. 5, the DOS distributions obtained with MPC and OPG have been adjusted so as to match in the CBT region. The capture coefficient(s) of the deep states is (are) probably different from that of the conduction band tail. In previous works, we have also found different capture coefficients between the deep states and the band tails,[13] what seems to be a characteristic of a-Si:H. From the present measurements, the difference between both capture coefficients seems to be a factor of the order of 3, which is the ratio of the DOS distributions deduced from OPG/MGT and MPC techniques in the energy range of 0.5–0.55 eV (see Fig. 5).

Finally, we have introduced as an input in our simulations the DOS and the transport parameters obtained from the OPG/MGT/MPC measurements. The DOS introduced in the simulations is presented in Fig. 6 (thick solid line), and is composed of a CBT having a characteristic temperature $T_C = 400$ K, and two Gaussian functions representing the deep states (dashed lines). The CBT and the Gaussian centred at 0.35 eV have capture coefficients $c_n = 4 \times 10^{-8}$ cm^3 s^{-1}, while the Gaussian centred at 0.60 eV has a capture coefficient $c_n = 1.2 \times 10^{-7}$ cm^3 s^{-1}. Introducing also the same experimental parameters of the measurements, like temperature range (130–390 K) and generation rate (2.5×10^{21} cm^{-3} s^{-1}), we have solved the transport equations and have computer-generated the OPG curves $\delta J(\omega)$, which were then treated as experimental data. We were able to reproduce quite accurately the general behaviour of our measurements. Indeed, the application of Eq. (12) to these data leads to the DOS reconstruction shown as circles in Fig. 6, and the application of Eq. (15) to the corrected values (valid for the CBT) shown as stars. Also, the solution of the MPC transport equations leads to the MPC-DOS shown as thin lines. If we compare with the experimental results of Fig. 5, we can see that all the features of the measurements are well reproduced.

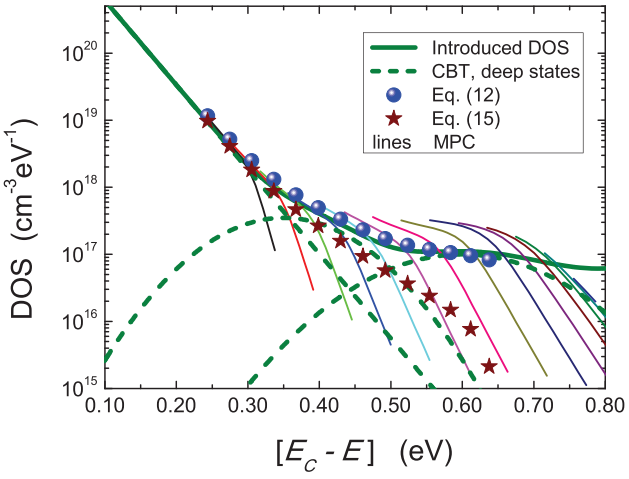

FIG. 6. DOS spectroscopies based on computer-generated data. The DOS used as a basis for the calculation (thick solid line) is shown decomposed in the CBT and the deep states (dashed lines). The thin lines are the results of the application of Eq. (16) to the MPC data, while the circles and the stars result from the application of Eqs. (12) and (15) to the OPG/MGT data, respectively.

From Fig. 5 or 6, it is apparent that the energy range covered by the MPC and OPG/MGT techniques is quite different. Because of the high flux needed to perform the OPG/MGT measurements in the lifetime regime, the position of the quasi-Fermi level is always rather high in the bandgap and it is difficult with this technique to get close to the dark Fermi level. To probe the midgap region, the temperature should be increased further or the dc flux should be decreased. Since we used light-soaked samples, we did not try to go to higher temperatures to avoid an annealing effect. However, even in the present conditions, the OPG/MGT method covers an interesting energy range between 0.22 and 0.58 eV from the conduction band edge (Fig. 5).

VI. CONCLUSION

We have described two characterisation techniques based on the measurement of the current resulting from the movement of an interference pattern onto the studied

sample. In one experiment, the moving grating technique, the pattern is moving at a constant velocity in one direction. In the other experiment, the oscillating photocarrier grating technique, the pattern is oscillating onto the sample, moving at a steady velocity in one direction during half a period of the driving frequency and in the other direction during the other half. The OPG technique can then be considered as an ac version of the MGT. However, from theoretical developments and numerical calculations, we have shown that the currents behaviours measured in both techniques have the same origin. We have then underlined that this property offers the possibility to use one technique or the other depending on the operational conditions and extends the range of fluxes and temperatures in which sample properties can be investigated. Indeed, we have demonstrated that with a proper treatment of the OPG/MGT data a density of states spectroscopy could be achieved performing these experiments at different temperatures. Two possible treatments have been proposed, a general one that can be applied to probe any distribution of states and a more refined treatment that is well suited for exponentially decreasing band tails. Finally, combining the results of these techniques with those of other experiments like MPC and SSPC, it is possible to derive good order of magnitude of the electron capture coefficient c_n of the conduction band tail states as well as the electron extended states mobility μ_n. We have applied all these experiments to some a-Si:H samples and found values of c_n and μ_n in good agreement with those found previously with a-Si:H samples studied with other techniques. OPG and MGT techniques can therefore be considered as useful techniques that provide good insight on some of the a-Si:H electronic transport parameters.

ACKNOWLEDGMENTS

This work was partly supported by ECOS-Sud under project A08E01. We thank the SOLSIA company for providing the a-Si:H samples.

APPENDIX: CALCULATION OF THE OPG EXCESS CURRENT DENSITY

We consider a sample built in coplanar geometry fitted with two ohmic parallel electrodes. An external electric field ξ_{ext} can be applied in between the electrodes. The illumination is made of two polarized laser beams of intensity I_1 and I_2, I_2 being smaller than I_1, say a tenth of I_1. The phase of one of the beams is modulated at an angular frequency ω by an electro-optic modulator that creates an oscillating grating. The two beams interfere on the sample, and the flux impinging it can be written

$$I(x,t) = I_0 + \delta I \cos(kx + \alpha\omega t), \tag{A1}$$

in which $k = 2\pi/\Lambda$, Λ being the grating period, $\delta I = \sqrt{I_1 I_2}$, $I_0 = I_1 + I_2$, t the time, $\alpha = \pm 1$ and x the position on the sample taken on an axis perpendicular to the electrodes.

The resulting generation rate in the sample can be written

$$G(x,t) = G_0 + \delta G \cos(kx + \alpha\omega t) = G_0 + \Re e[\delta G\, e^{jkx+\alpha j\omega t}], \tag{A2}$$

in which $G_0 = G_1 + G_2$, G_1 resulting from I_1 and G_2 resulting from I_2, and $j^2 = -1$.

For simplicity, the following calculation will assume that only a single species of monovalent states is present in the band gap of the material and we shall use the notations of the paper.[13] It can be shown that considering the presence of different species of dangling bonds and monovalent states does not modify the general line of the calculation but it would be too long to give the complete calculation.

Locally, the electric field can be decomposed in two components, the externally applied field ξ_{ext} and a local field ξ_{int}. The neutrality equation can be written, taking into account of thermal equilibrium (indexes 0)

$$\frac{d\xi_{\text{int}}(x,t)}{dx} = \frac{q}{\varepsilon\,\varepsilon_0}\left\{p(x,t) - p_0 - n(x,t) + n_0 - \int_{E_v}^{E_c}[f(E,x,t) - f_0]N(E)dE\right\}. \tag{A3}$$

The continuity equations are

$$\frac{\partial n}{\partial t} = G(x,t) - R_n(x,t) + \mu_n \frac{d}{dx}[n(x,t)\,\xi(x,t)] + D_n \frac{d^2 n(x,t)}{dx^2}, \tag{A4}$$

$$\frac{\partial p}{\partial t} = G(x,t) - R_p(x,t) - \mu_p \frac{d}{dx}[p(x,t)\,\xi(x,t)] + D_p \frac{d^2 p(x,t)}{dx^2}, \tag{A5}$$

with the recombination terms

$$R_n(x,t) = \int_{E_v}^{E_c}\{c_n n(x,t)[1 - f(E,x,t)] - e_n(E) f(E,x,t)\}N(E)dE, \tag{A6}$$

$$R_p(x,t) = \int_{E_v}^{E_c}\{c_p p(x,t) f(E,x,t) - e_p(E)[1 - f(E,x,t)]\}N(E)dE, \tag{A7}$$

and

$$\frac{\partial f(E,x,t)}{\partial t} = c_n n(x,t) + e_p(t) - f(E,x,t)[c_n n(x,t) + e_n(t) + c_p p(x,t) + e_p(t)]. \tag{A8}$$

Following the complex expression of the generation rate, most of the quantities can be written $Q = Q_0 + \Delta Q e^{j\alpha\omega t} e^{jkx}$ and one has for the states occupancy

$$\frac{\partial f(E,x,t)}{\partial t} = c_n(n_0 + \delta n e^{j\alpha\omega t}e^{jkx}) + e_p - (f_0 + \delta f e^{j\alpha\omega t}e^{jkx}) \times \left\{ c_n(n_0 + \delta n e^{j\alpha\omega t}e^{jkx}) + e_n + c_p(p_0 + \delta p e^{j\alpha\omega t}e^{jkx}) + e_p \right\} \tag{A9}$$

and $\frac{\partial f(E,x,t)}{\partial t} = j\alpha\omega\delta f e^{j\alpha\omega t}e^{jkx}$, which leads to

$$\delta f = \left(\frac{c_n\delta n(1-f_0) - c_p\delta p f_0}{\frac{1}{\tau} + j\alpha\omega} \right), \tag{A10}$$

in which one has $\frac{1}{\tau} = c_n n_0 + c_p p_0 + e_n + e_p$.

If one writes $\delta n = n_r + \alpha j n_i$ and $\delta p = p_r + \alpha j p_i$, then one ends with a system of equations

$$\begin{aligned} A_n n_r - B_n n_i + A_p^* p_r + B_p^* p_i &= \delta G \\ B_n n_r + A_n n_i - B_p^* p_r + A_p^* p_i &= 0, \\ A_n^* n_r + B_n^* n_i + A_p p_r - B_p p_i &= \delta G, \\ -B_n^* n_r + A_n^* n_i + B_p p_r + A_p p_i &= 0. \end{aligned} \tag{A11}$$

The expressions of the coefficients of the system (A11) can be written

$$A_n = k^2 D_n + M_n\left(1 + \int_2^n\right) + A_n^{mpc}, \qquad A_p = k^2 D_p + M_p\left(1 + \int_2^p\right) + A_p^{mpc},$$

$$B_n = -\mu_n k\alpha\xi_{ext} - M_n\omega\int_3^n + B_n^{mpc}, \qquad B_p = \mu_p k\alpha\xi_{ext} - M_p\omega\int_3^p + B_p^{mpc},$$

$$A_n^* = -M_p\left(1 + \int_2^n\right) + A_n^{*mpc}, \qquad A_p^* = -M_n\left(1 + \int_2^p\right) + A_p^{*mpc},$$

$$B_n^* = -M_p\omega\int_3^n + B_n^{*mpc}, \qquad B_p^* = -M_n\omega\int_3^p + B_p^{*mpc},$$

where the coefficients with a superscript *mpc* are those found in a previous paper concerning this technique [see for instance Ref. 7, being careful that the notations are not the same in both papers, the * being shifted for the A_p and B_p coefficients], and with $M_n = n_0\mu_n\frac{q}{\varepsilon\varepsilon_0}$, $M_p = p_0\mu_p\frac{q}{\varepsilon\varepsilon_0}$, $M_n + M_p = 1/\tau_D$, τ_D being the dielectric relaxation time. Besides, the integrals are written as

$$\int_2^n = \int c_n\frac{(1-f_0)\tau N(E)}{1+\omega^2\tau^2}dE, \qquad \int_3^n = \int c_n\frac{(1-f_0)\tau^2 N(E)}{1+\omega^2\tau^2}dE,$$

$$\int_2^p = \int c_p\frac{f_0\tau N(E)}{1+\omega^2\tau^2}dE, \qquad \int_3^p = \int c_p\frac{f_0\tau^2 N(E)}{1+\omega^2\tau^2}dE.$$

The reader may note that in the above expressions one has to take $\alpha\xi_{ext}$ into account and not simply ξ_{ext}. All the integrals are taken between E_v and E_c, the energies of the top of the valence and bottom of the conduction bands, respectively.

Solving the system (A11) provides expressions for n_r, n_i, p_r, and p_i. These expressions are rather heavy and we shall not provide them here. As in Ref. 18, the current density is given by

$$J_{coh} = \frac{1}{\Lambda}\int_0^\Lambda [q\,\mu_n n(x) + q\mu_p p(x)]\,[\xi_{ext} + \xi_{\text{int}}(x)]\,dx = J_0 + \delta J,$$

$\xi_{int}(x)$ can be calculated from Eq. (A3) and one has

$$\xi_{\text{int}}(x) = \Re e\left\{ -\frac{jq}{\varepsilon\varepsilon_0 k}\left[\delta p - \delta n - \int \delta f N(E)dE\right]\exp(jkx + j\alpha\omega t)\right\},$$

and

$$\sigma = q[\mu_n n_0 + \mu_p p_0] + \Re e\Big(q[\mu_n\delta n + \mu_p\delta p]\exp(jkx + j\alpha\omega t)\Big),$$

the expression of δJ is given by $\delta J = \Re e(\delta\bar{\sigma})\Re e(\bar{\xi}_{\text{int}})$ and can also be calculated from $\delta J = {}^1\!/_2\,\Re e(\delta\bar{\sigma}^*\bar{\xi}_{\text{int}})$, in which $\delta\bar{\sigma}^*$is the conjugated complex of $\delta\bar{\sigma}$. It gives

$$\delta J = {}^1\!/_2\,\Re e\left(-\frac{jq^2}{\varepsilon\varepsilon_0 k}\left[\delta p - \delta n - \int \delta f N(E)dE\right][\mu_n\delta n^* + \mu_p\delta p^*]\right). \tag{A12}$$

If one introduces the expressions of Δn, Δp and Δf in this expression (A12) and writing $\Delta\bar{\sigma}$ and $\bar{\xi}_{\text{int}}$ as $\delta\bar{\sigma} = \sigma_r + \alpha j\sigma_i$ and $\bar{\xi}_{\text{int}} = \xi_r + j\alpha\xi_i$ one ends with

$$\delta J = \alpha\frac{1}{2}(\xi_r\sigma_r + \xi_i\sigma_i), \tag{A13}$$

with

$$\sigma_r = q(\mu_n n_r + \mu_p p_r), \quad \sigma_i = q(\mu_n n_i + \mu_p p_i), \tag{A14}$$

$$\xi_r = \frac{\alpha q}{\varepsilon\varepsilon_0 k}\left[p_i\left(1 + \int_2^p\right) - n_i\left(1 + \int_2^n\right) - p_r\omega\int_3^p + n_r\omega\int_3^n\right], \tag{A15}$$

$$\xi_i = -\frac{\alpha q}{\varepsilon\varepsilon_0 k}\left[p_r\left(1 + \int_2^p\right) - n_r\left(1 + \int_2^n\right) + p_i\omega\int_3^p - n_i\omega\int_3^n\right]. \tag{A16}$$

Some simplifications can be done in the expressions (A14)–(A16) if we assume that the external field is equal to zero and if one performs the experiment with large grating period leading to small k value. Finally, we end with

$$\xi_r = \frac{\alpha q}{\varepsilon\varepsilon_0 k}\left[-\frac{k^2 D_n\tau_D}{1+(\omega\tau_D)^2}(-n_i^{mpc} + \omega\tau_D n_r^{mpc}) + \frac{k^2 D_p\tau_D}{1+(\omega\tau_D)^2}(-p_i^{mpc} + \omega\tau_D p_r^{mpc})\right],$$

$$\xi_i = \frac{\alpha q}{\varepsilon\varepsilon_0 k}\left[-\frac{k^2 D_n\tau_D}{1+(\omega\tau_D)^2}(n_r^{mpc} + \omega\tau_D n_i^{mpc}) + \frac{k^2 D_p\tau_D}{1+(\omega\tau_D)^2}(p_r^{mpc} + \omega\tau_D p_i^{mpc})\right].$$

If we take only into account the electron contribution then we have, from Eq. (A13)

$$\delta J(\omega) = \mp\frac{k^2\frac{k_BT}{q}\omega\tau_D^2}{1+(\omega\tau_D)^2}\frac{q^2}{2\varepsilon\varepsilon_0 k}\mu_n^2(n_r^{mpc^2} + n_i^{mpc^2}),$$

that is,

$$\delta J(\omega) = \mp\frac{k\frac{k_BT}{q}}{1+(\omega\tau_D)^2}\frac{\sigma_{mpc}^2}{2\sigma_{ph}^2}\omega\varepsilon\varepsilon_0. \tag{A17}$$

[1]R. Brüggemann, J. Appl. Phys. **92**, 2540 (2002).
[2]S. K. Ram, S. Kumar, and P. Roca I. Cabarrocas, Thin Solid Films **515**, 7576 (2007).
[3]A.Rose in *Concepts in Photoconductivity and Allied Problems* (John Wiley, New York, 1963), Chap. 2.
[4]C. Main, S. Reynolds, and R. Brüggemann, Phys. Status Solidi C **1**, 1194 (2004).
[5]H. Oheda, J. Appl. Phys. **52**, 6693 (1981).
[6]R. Brüggemann, C. Main, C. Berkin, and J. Reynolds, Philos. Mag. B **62**, 29 (1990).
[7]C. Longeaud and J. P. Kleider, Phys. Rev. B **45**, 11672 (1992)
[8]D. Ritter, E. Zeldov, and K. Weiser, Appl. Phys. Lett. **49**, 791 (1986).
[9]K. Hattori, Y. Koji, S. Fukuda, W. Ma, H. Okamoto, and Y. Hamakawa, J. Appl. Phys. **73**, 3846 (1993).
[10]U. Haken, M. Hundhausen, and L. Ley, Appl. Phys. Lett. **63**, 3063 (1993).
[11]F. Ventosinos, N. Budini, C. Longeaud, and J. A. Schmidt, J. Phys. D: Appl. Phys. **44**, 295103 (2011).
[12]C. Longeaud, J. A. Schmidt, and R. R. Koropecki, Phys. Rev. B **73**, 235317 (2006).
[13]C. Longeaud, J. A. Schmidt, R. R. Koropecki, and J. P. Kleider, J. Optoelectron. Adv. Mater. **11**, 1064 (2009).
[14]F. Ventosinos, C. Longeaud, and J. A. Schmidt, "Density of states evaluations from oscillating/moving grating techniques," J. Non-Cryst. Solids (in press).
[15]Y. Li, Phys. Rev. B **42**, 9025 (1990).
[16]G. W. Taylor and J. G. Simmons, J. Non-Cryst. Solids **8–10**, 940 (1972).
[17]C. Longeaud, D. Roy, and O. Saadane, Phys. Rev. B **65**, 085206 (2002).
[18]J. A. Schmidt and C. Longeaud, Phys. Rev. B **71**, 125208 (2005).